# Drop Volume Modulation via Applied Backpressure in Inkjet Systems

***Aaron Fulton, J. William Boley, Nikhil Bajaj, and George T.-C. Chiu***
***School of Mechanical Engineering, Purdue University, West Lafayette, Indiana 47907***

## Abstract

*To date, there are limited options in the ability to create droplets of smaller radii than that of the nozzle from which they are produced. Existing methods pertain largely to piezoelectric inkjet printing and time scale manipulation rendering them inapplicable to thermal inkjet technologies. In this work, a simple method for drop volume control in inkjet systems is proposed in which stable drop volume can be reduced by an order of magnitude with a constant nozzle radius by adjusting the back pressure in the reservoir that supplies the print head. The back pressure is regulated, droplet sizes, stability, and velocities are recorded. These results are then corroborated by rigorous modeling.*

## Introduction

In functional inkjet printing applications, it may be desirable to enable tuning of the dot gain to accommodate multiple size scales within a device at a high throughput. This becomes an issue when printing large space filling areas and small features within the same device, such as in a comb capacitor. The capacitive elements require thin lines where a small drop volume is necessary, while the contact pads require a larger area, where a large drop volume would optimize throughput. To date there are limited options in the ability to modulate drop volume with a single nozzle. Existing methods pertain to piezoelectric inkjet printing, which control the waveform and time scale manipulation of the capillary, viscous, and inertial flow behavior, rendering them inapplicable to traditional thermal inkjet technologies [8-9]. Specifically, the waveform manipulation used to create smaller droplets is a departure from the traditional square waveform, and cannot be replicated by thermal inkjets. It is this difference that currently acts to limit inkjet drop volume modulation. A novel method for simple drop volume control in thermal inkjet systems is proposed in which stable drop volume can be reduced by an order of magnitude with a constant nozzle radius. It is shown that the key to forming drops with radii smaller than that of the nozzle is to adjust the back pressure in the reservoir that supplies the print head.

To determine the extent and nature of the effect of high backpressure, the back pressure is regulated through the use of a syringe, and measured throughout the printing process and droplet masses and velocities are found. To form a complete model of this phenomena the data for these tests are collected through a range of heights, pressures, and fluids, and evaluated for droplet quality and satellite formation. These results are justified through theoretical and numerical analysis [7-9, 16], leading to a view that this phenomena is driven by meniscus shaping, driving waveform, inkjet geometry, and fluid properties. Additionally the results are subjected to traditional non-dimensional analysis for prediction of droplet stability and droplet sizing through a numerical methods parameter sweep and compared to similar results [7-9].

## Experimental details

### *System*

All physical experiments were performed with a HP TIPS system with a nozzle diameter of 67μm, with a voltage input of 29V with a pulse width of 3.1μs. The back pressure for all data points was recorded via an internal pressure sensor in the TIPS controller at the instance of each firing, and the control of pressure was achieved through the use of a syringe. The nozzle is primed before the printing of any pattern by forcing a small amount of fluid out of the nozzle using the syringe then pulling back any excess then wiping the print head clean of any remnants. The Pd ink and SU-8 underwent the same waveforms and procedures for all tests. A minimum temperature and maximum temperature of 22 and 26 degrees Celsius was held throughout all printings.

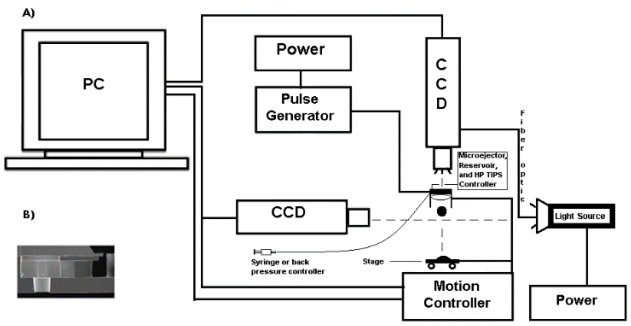


**Figure 1:** Experimental Setup, and generic nozzle profile of TIPS Nozzle, scale withheld and image distorted

### *Drop Volume Experiments*

To find the average mass of the droplet, 432,000 droplets were deposited on a pre-weighed piece of aluminum foil and allowed to dry for 24hrs in 60 layers of a 60 by 120 dot matrix. A single nozzle with a slow firing frequency of 1000Hz was used to avoid cross talk, however, slower than this could promote clogging, and as such the long period of printing could be prone to failure to fire events. Additionally, this process was actively watched continuously for trends or clogging. These then were measured and using ink data allowed for statistical estimation of the average droplets produced.

### *Drop Speed Experiments*

To find the droplet velocity we utilized the method of bidirectional printing with varied heights [5]. This test consisted of multiple single column target print patterns, printed bi-directionally at high scanning speeds, $U_{scan}$, with known standoff distances between the print head and the substrate. Since there was time delay, $\tau$, between the trigger pulse and when the droplet

impact on the substrate, the actual deposition position of every droplet had either some translation correlating to the lead or lag and the true trigger position depending on the print scan direction. The distance, $d$, between the two columns of dots was found by subtracting the centroid positions of the drops in each column through image processing algorithms in MATLAB using a circular Hough transform. The time delay, τ, was then found for each respective back pressure and height combination using these images,

$$\tau = \frac{d}{2U_{scan}}, \tag{1}$$

where $U_{scan}$ was the highest stage speed of 225mm/s and the stand-off distances ranged between .3mm and 2.1mm. Assuming drop speed changes minimally throughout the flight time, the impact velocity is the slope of delay against standoff distance. This also served as a method for satellite detection as the high stand-off distance and speeds would exacerbate satellite trajectory differences and increase offset on the substrate. To examine the possibility of a frequency of fire limiting phenomena we simply attempted to print patterns on parafilm with as tight a pixel pitch as possible while using the maximum speed of the stage, $U_{scan}$. This gave the ability to check for fire while refilling or failure to fire visually via qualitative checks between speeds, at a set backpressure. Visual recognition code recognizes satellites and reports their size, number, and their respective centroids using similar methods.

## Simulation Details

To understand the phenomena seen in the thermal inkjet system, we examined the same phenomena in a well-defined piezoelectric inkjet system. Comparable results were obtained when using level set and phase field methods when sufficiently tight meshing was applied; the results for phase field are presented. In the phase field module, the interface dynamics of the two-phase flow is governed by a Cahn-Hilliard equation, which tracks a diffuse interface separating the phases. We ignore phase changes across the interface as the droplets are large enough that through the analysis outlined by Boley in 2009 [3]. We can determines that the evaporation is less than 1% of the total volume within the flight time shown. Accordingly, for the shown simulation the volume fraction is found to be

$$V_f = \frac{1+\phi}{2}, \tag{2}$$

where $\phi$ is the dimensionless phase variable; varying between -1 and 1. The density, $\rho$, $(kg \cdot \mathrm{m}^{-3})$ and the viscosity, $\eta$, $(Pa \cdot s)$ of the fluid are smoothly varied across the interface via,

$$\rho = \rho_{gas} + (\rho_{fluid} - \rho_{gas})V_f, \tag{3}$$

$$\eta = \eta_{gas} + (\eta_{fluid} - \eta_{gas})V_f. \tag{4}$$

Relating the surface tension to interface thickness yields,

$$\sigma = \frac{2^{\frac{3}{2}} \cdot \lambda}{3 \cdot \varepsilon}, \tag{5}$$

where surface tension, σ $(\mathrm{N} \cdot \mathrm{m}^{-1})$, to interface thickness, ε (m). Cahn-Hilliard equation tracks the diffuse interface separating immiscible phases. The diffuse interface is defined as the region where the dimensionless phase field variable goes from −1 to 1. This describes the process of phase separation, by which the two components of an immiscible binary fluid spontaneously separate. The Cahn-Hilliard equation is a fourth-order equation, so posing it in its weak form would result in the presence of second-order spatial derivatives, and the problem could not be solved using a standard Lagrange finite element basis. The solution is to rephrase the problem as two coupled second-order equations. In COMSOL the Cahn-Hilliard equation is dealt with by this implementation of these two coefficient form PDEs in time discrete form,

$$\frac{\partial \phi}{\partial t} + \boldsymbol{u} \cdot \nabla \phi = \nabla \cdot \frac{\gamma \lambda}{\varepsilon^2} \nabla \Psi, \tag{6}$$

$$\Psi = -\nabla \cdot \varepsilon^2 \nabla \phi + (\phi^2 - 1)\phi\,, \tag{7}$$

where $\gamma$ is the species mobility$(m^3 \cdot s \cdot kg^{-1})$, $\boldsymbol{u}$, is the fluid velocity$(m/s)$, $\lambda$ is the mixing energy density $(N)$, and, ε, the interface thickness (m). The initial guess relating the mobility and interface thicknesses was determined to be sufficient at the traditional initial guess,

$$\gamma = \varepsilon^2. \tag{8}$$

The liquid velocity field in the reservoir and the droplet velocity field are described by the incompressible Navier-Stokes equation as the velocity of both fluids is assumed to be well below both of their respective speeds of sound,

$$\rho\left(\frac{\partial \boldsymbol{u}}{\partial t} + \boldsymbol{u} \cdot \nabla \boldsymbol{u}\right) - \nabla \cdot \left(\mu(\nabla \boldsymbol{u} + \nabla \boldsymbol{u}^{\boldsymbol{T}})\right) + \nabla \mathrm{p} = F_{st}\,, \tag{9}$$

$$\nabla \cdot u = 0. \tag{10}$$

Phase field uses the diffuse interface to compute surface tension as,

$$F_{st} = G\nabla\phi. \tag{11}$$

The chemical potential, G$(\frac{J}{m^3})$, can be seen as,

$$G = \lambda \frac{1}{\varepsilon^2} \Psi = \lambda[-\nabla^2\phi + \frac{\phi(\phi^2-1)}{\varepsilon^2}]\,. \tag{12}$$

Accordingly, the surface tension for this particular simulation is an interfacial force distribution in respect to the gradient and dimensionless phase field variable. All fluid properties used in analysis and simulation were determined experimentally[20] with the notable exception of the viscosity of Pd ink which was determined through the empirical relation found by both the relation found by Thomas in 1965 and Einstein's equations found in 1906 for effective viscosity for dilute solutions of fine particles,

$$\mu_s = \mu_r \cdot \mu_l, \tag{13}$$

$$\mu_r = 1 + 2.5 \cdot \phi_s + 10.05 \cdot \phi_s + 0.00273 \cdot e^{16.6 \cdot \phi_s}, \tag{14}$$

$$\mu_r = 1 + 2.5 \cdot \phi_s, \tag{15}$$

where $\mu_s(Pa \cdot s)$ is the dilute solution viscosity, $\mu_l$ is the solute viscosity, $\mu_r$ reflects the particulate contribution to the relative solute, and $\phi_s$ is the volume fraction of solid particulate. With these we found values within 5% of each other due to low volume fractions of particles; the Thomas correlation is used for all further work. Using these we determined the Weber, Reynolds, Capillary, Bond, and Ohnesorge numbers. All simulations performed were accomplished using COMSOL Multiphysics, in recreation of prior simulation of experimental phenomena [7]. To compare the results

of experiment and simulation to previous work nondimensional analysis for the printability regime was performed

$$Re = \frac{u\rho L}{\mu_s} = \frac{Inertial\ Effects}{Viscous\ Effects}, \quad (16)$$

$$We = \frac{\rho u^2 L}{\sigma} = \frac{Inertial\ Effects}{Capillary\ Effects}, \quad (17)$$

$$Ca = \frac{We}{Re} = \frac{Viscous\ Force}{Capillary\ Force}, \quad (18)$$

$$Oh = \frac{\sqrt{We}}{Re} = \frac{Viscous\ Forces}{\sqrt{inertia \cdot surface\ tension}}, \quad (19)$$

$$Bo = \frac{\rho g L^2}{\sigma}, \quad (20)$$

where ρ is the density of the fluid($Kg \cdot m^{-3}$), u is its velocity ($m \cdot s^{-1}$), L is the characteristic length, typically the droplet diameter (m), σ is the surface tension ($N \cdot m^{-1}$). The parameters that control the effects of the backpressure are dependent of viscosity, surface tension, driving waveform, density, refill dynamics, geometry, and nozzle size. A plotting of this region in this parameter space has only been only created in regions directly comparable to other regions in literature.

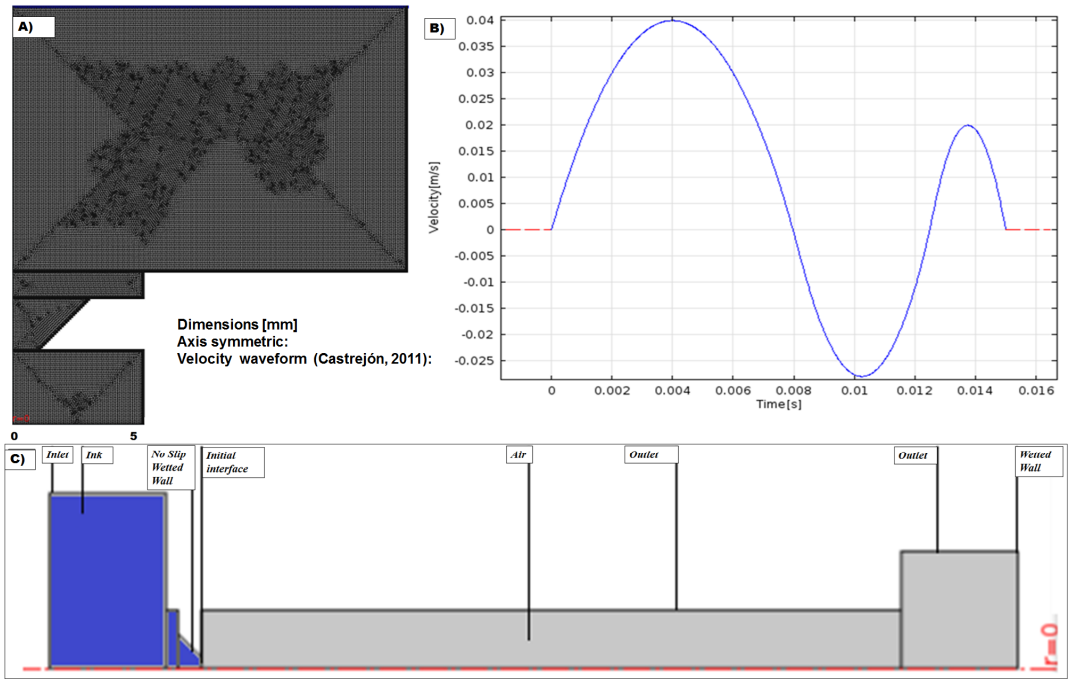


***Figure 2.*** *Recreation of Castrejón-Pita in 2011 and adaptations of simulations: A) Extremely fine physics based meshing in COMSOL, lagrangian meshing with an initially even distribution of elements, the initial number of elements was 4,320, adaptive meshing however so this change based upon the movement of the interface: initial number of elements for extremely fine physics based meshing for this geometry was, B) Velocity input waveform [7], C) Diagram of simulation properties.*

The results of the original experiment and simulation were first found through fine tuning of the system while using phase field methods, this result was then used to verify the accuracy of the simulation. DOD droplet formation for a glycerol-water mixture was simulated and compared with the results obtained by Castrejon -Pita in 2011, where the density, viscosity, and surface tension of the glycerol-water mixture are 1222 $Kg \cdot m^{-3}$, 0.1 $Kg \cdot m^{-1} \cdot s^{-1}$, and 0.064·N· $m^{-1}$, respectively. Back pressure was then applied to two levels with an assumed receding contact angle of 5° to obtain a clear trend. The droplet is examined for speed, volume, splashing, and satellites, then lands on a piece of glass and is examined. There was use of up to 40% adjustment in the driving forms amplitude and this was tuned to achieve the closest results possible. All meshing was automatically done using the tightest physics based meshing. The back pressure is applied for 40 milliseconds for pseudo-equilibrium at which point the waveform is applied to the inlet at which point the droplet is ejected traditionally. This numerical experiment is performed for a variety of fluid properties. In Figure 2, boundary conditions and applied meshing, piezoelectric waveform as found experimentally [7] and assumed ejection and refill generic characteristic waveform to examine the effects of short high amplitude input.

## Results

To experimentally investigate the phenomena connect backpressure modulation, two relatively differing fluids were jetted and observed. The fluids were SU-8 2002 and Palladium hexadecane thiolate ink (Pd ink) with a concentration of 47400$kg \cdot m^{-3}$ in toluene were used. In the case of the Pd ink, by using the average drop mass measurement one can obtain a maximum average droplet diameter of 65.18μm and an average minimum of 25μm at average pressures of 287 Pa and 9247 Pa respectively. Additional tests for SU-8 2002 yielded similar results as the diameter decreased in a nearly linear fashion with higher back pressure creating satellites

*Table 1: All values reported [20], with notable exceptions of SU-8 2002 and Palladium hexadecane thiolate in toluene, eq.13-14, [22]*

| Fluid Properties | Surface Tension ($N \cdot m^{-1}$) | Viscosity ($Pa \cdot s$) | Density ($kg \cdot m^{-3}$) |
|---|---|---|---|
| SU-8 2002 | 0.048 | 0.0084225 | 1123 |
| Palladium Hexadecane Thiolate | 0.0243 | 0.00060275 | 873.3 |
| Toluene | 0.0284 | 0.00059 | 866.9 |
| Ethanol | 0.02239 | 0.00104 | 789 |
| Acetone | 0.0211 | 0.00395 | 802.5 |
| Water | 0.07199 | 0.00089 | 997.04 |
| Ethylene Glycol | 0.024 | 0.0003311 | 791 |
| Isobutanol | 0.0211 | 0.00395 | 802.5 |

## Experimental

To compare these to the apparent diameter of the droplets deposited optically we assume the droplet formed with no back pressure to have a diameter comparable to that of the nozzle preceding impact. We then determine the diameter based upon wetting dynamics and capillary spreading being of a longer time scales than the initial spreading and contractions and shorter than evaporation [5]. A droplet of Pd ink with a back pressure of 9000 Pa has a diameter of roughly 28μm [11]. Similar results were found with all other inks and using several nozzles of the same type. Backpressures for SU-8 are only shown from 1000 Pa to 7000 Pa. This is because satellites are formed from 7000 Pa through 8500 Pa for the same driving waveform as used for the Pd ink. By reducing the input waveform amplitude from 29V to 28.92V stable droplets could be created. In experiments using Pd ink, a back pressure of 10500Pa would yield satellite droplets similarly to SU-8. A reduction in voltage from 29V to 28.92V yielded fully stable droplets when printing patterns at 1 kHz. Further reduction of voltage input lead to a situation where unstable droplets were not creatable but rather a no fire event was reached. This stands to support simulation results, and demonstrates a considerable range increase from that of a square wave input. When evaluating results in must be noted [17] that there is a relatively dissimilar Bond number

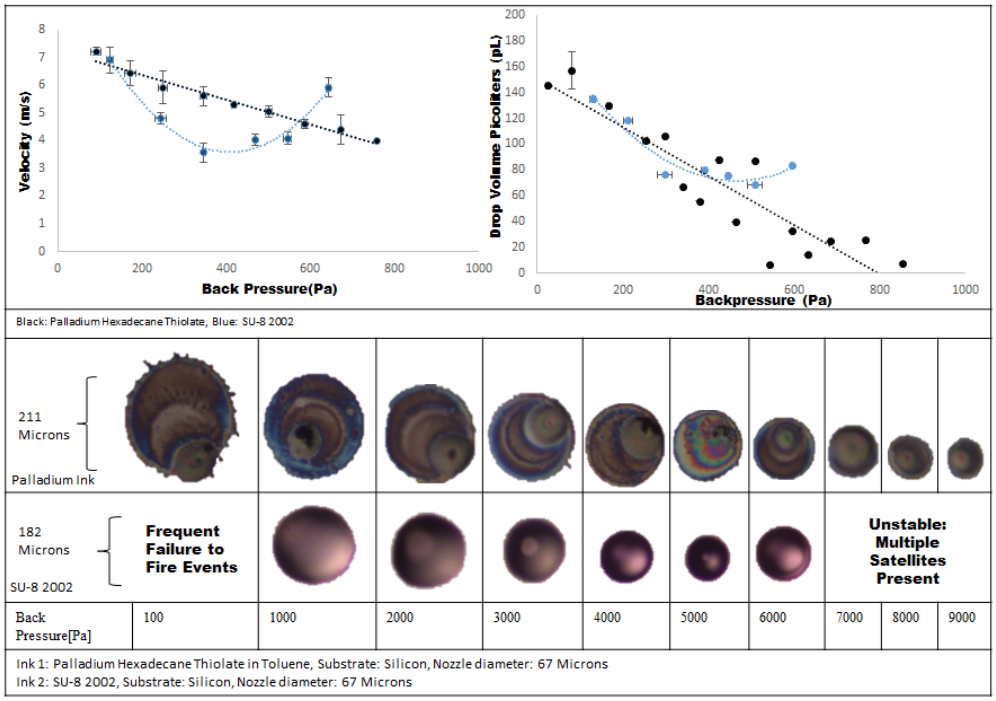


***Figure 3.*** *Experimental: Pd toluene(black)), SU-8 2002(blue),estimated drop volume as a function of back pressure. Drop volume decreases nearly linearly with increased back pressure. (Note: in picture of droplet deposited show what appears to be splash marks, while possibly splashing, these have previously been found to be a result of drop morphology of larger droplets due to Marangoni flows being stronger in the larger volume of fluid, these accordingly get smaller as the droplet gets smaller reducing the effect [4])). Droplets shown were found to be close to the statistical average diameter as deposited on polished silicon, SU-8 2002 tends to polymerize during flight at increasing rates and times as the drop volume decreases and length increases, respectively this rendered comparison between deposited droplets and droplets in flight difficult as the spreading dynamics are subject to change in respect to height of deposition and size and as such are all shown from the lowest height of .3mm. Additionally, droplet deposition was unsustainable as there was leaking and clogging at backpressures below 1000Pa and are accordingly not represented. Lastly, a trend in droplet production was that upon incurring satellites the fluid volume ejected is reduced, including satellites, again as the upswing is reversed this is reflected in dot gain of the primary droplet.*

## Simulation

Simulation gave a qualitative and quantitative approach towards determining the effects of backpressure. The primary effect can be seen as three distinct effects working in conjunction to reduce drop volume. The first effect is that as the energy to eject the droplet increases as the size of the meniscus increases, a reduction in input energy decreases droplet volume linearly to a point [16]. In practice, this marginally narrows the profile and suppresses the expansion of the droplet. However, the nature of the effect of back pressure on drop volume is based on the suppression of droplet growth along the sides due to inertia of the fluid in the meniscus and the collapse of the meniscus. As such, the other effect that further exacerbates this reduction in volume is the horizontal collapse of the meniscus due to channeling of the fluid along the

angled sides causes the formation of a Worthington jet [8]. This causes a sharp profiled jet to protrude from the already narrowed column of fluid. A sharper angle would incur a more aggressive collapse. As the meniscus acts to narrow the jet, we achieve an almost sharp and pointed profile, and this profile then continues to expand. This jet then becomes unstable and breaks up leaving a droplet far smaller in diameter than the. Lastly, the fluid must move through additional space to exit the nozzle and accordingly is not given the same amount of time to grow and lengthen before the refill oscillations begin. This reduces aspect ratio of the column ejected and showed attributes similar in nature to those previously expressed [2, 8].

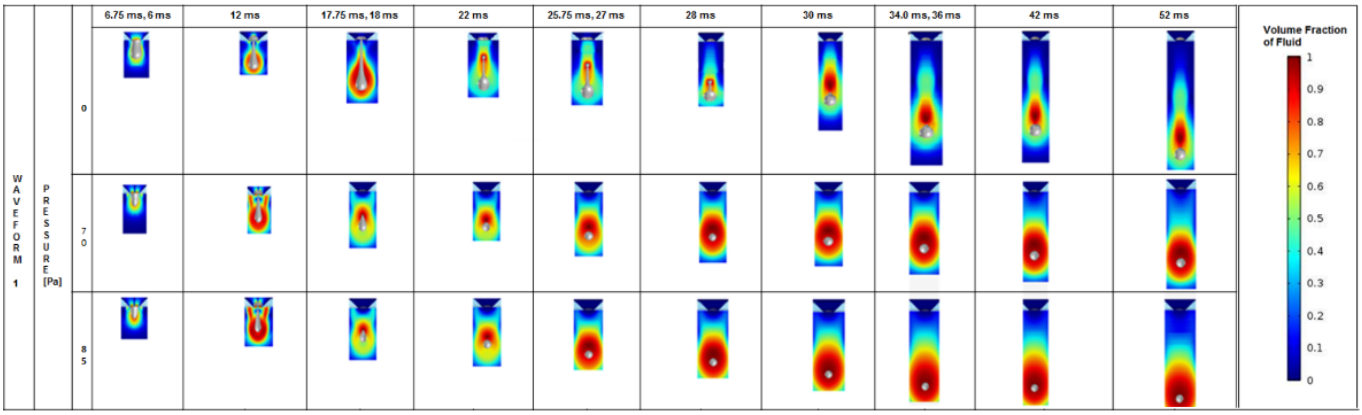


***Figure** 4. Simulation confirmation, applied waveforms, applied backpressures, geometry, 1st row results compared [7], 2nd and 3rd row illustrate effects of back pressure using the same waveform as found by Castrejón-Pita and as seen in the 0Pa row above, 4th row illustrates modified waveform, waveform 1 as seen in experimental setup. Numerically it was determined that the drop diameter for the simulation of this waveform with no back pressure was 2.158mm. However, with a back pressure of 70Pa the diameter was reduced by 4% to 1.38mm accordingly the drop volume was reduced by 74.9%. Additionally, when the modified waveform was applied the droplet diameter was further reduced by 52.5% to 1.05mm and droplet volume decreased by 86.6%.*

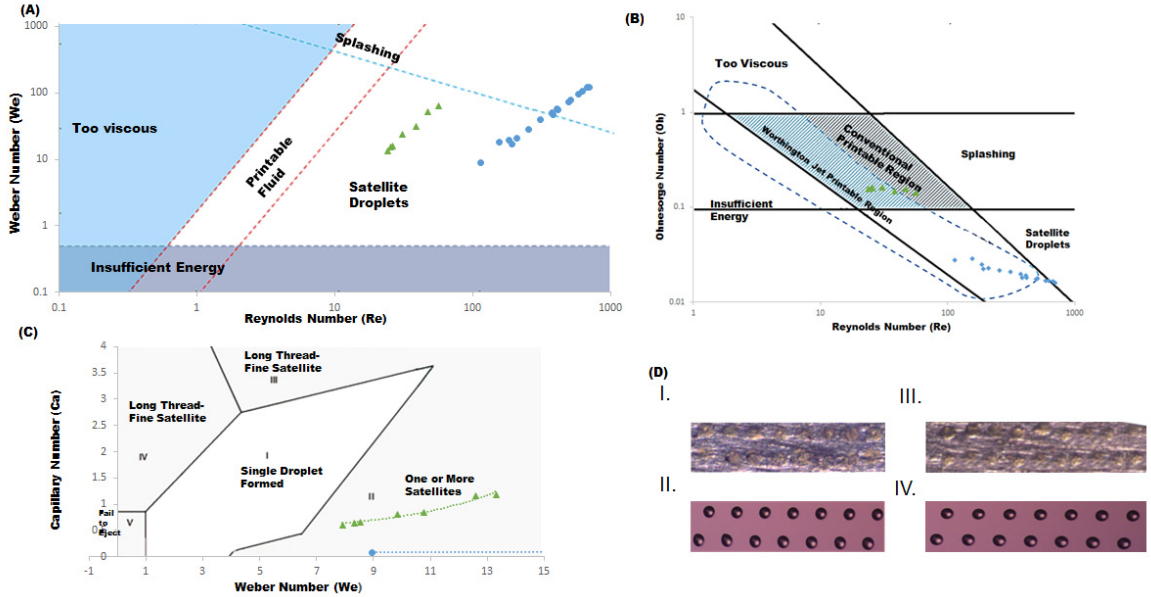


***Figure 5.** A) Toluene: blue: SU-8: green: Comparison to printable region diagram [8], B) Reynolds vs. Ohnesorge Reynolds numbers, comparison to printable region diagram[10], C) comparison to printable region diagram [17], D) I. Frequency to fire at back pressure 750Pa, standoff distance of .6mm, firing waveform 29V with duration of 3.1μs: I.100Hz firing frequency with Pd in with a backpressure of 750Pa, II. 100Hz firing frequency with SU-8 2002 with a backpressure of 500Pa, III. 2000Hz firing frequency with Pd ink with a backpressure of 750Pa, IV. 1500Hz firing frequency with SU-8 2002 with a backpressure of 500Pa.*

## *Stability*

Throughput is always a primary concern when evaluating functional inkjet printing. For the TIPS 23 the maximum firing frequency for de-ionized water is 4 kHz, however, the suggested frequency for all fluids is less than 2 kHz as this prevents fire during refill as well as the coincidental heating of the die which can degrade functional inks and change fluid properties considerably. Accordingly we tested the system at a maximum frequency with Pd ink in toluene achieving a maximum firing frequency, as restricted by spacing and stage velocity, of 1184.21 Hz and 2045 Hz at 100 Pa and 750 Pa respectively with minimal degradation of quality, no satellites, and no observed failure to fire events, when compared to lower frequencies. This method produces a similar range in stable droplets to that seen in Castrejón-Pita's work in 2012 within 2 kHz firing frequency. While there is an intuitive reduction in refill speed with increased back pressure, this data shows that the effect of high

backpressure does not significantly reduce the maximum firing frequency as other factors such as die heating or droplet morphologies may restrict it first. Additionally, all alternative piezoelectric pressure waveforms used to reduce droplet size involve a preconditioning negative impulse that is then either removed allowing for collapse [8] or a positive impulse is sent forcibly collapsing the meniscus [9]. This type of waveform also decreases maximum frequency of fire in all inkjet systems.

## Conclusion

Throughput, small feature size, and increased printing range are paramount in the world of functional printing. Back pressure-based meniscus manipulation allows for potential increase in performance in all three of these factors. While there exist several methods in literature that can accomplish these improvements, they are not implementable across several types of printing, specifically thermal inkjet. The effect is primarily driven by three factors: meniscus size, geometry, and waveform. While other factors play into droplet modulation, such as fluid properties and rheology, it is these three that can in certain fluid systems reduce drop size and increase the printing ranges with regards to fluid properties, size, and velocity. Through appropriate control of these factors it is possible tune the back pressure, passively or actively to achieve smaller sizes from larger nozzles. As a result one might be able to change print mask designs for increased efficiency, and deposit fluids at speeds and in sizes potentially unreachable by traditional methods of printing. Additionally, the method of backpressure control is potentially usable across platforms. This allows for ease of incorporation of this technique. Active backpressure control is a practical, effective, and inclusive method by which one can modulate drop size and velocity and increase printability range in a variety of fluids when using inkjet system

***Acknowledgements***

The authors would like to thank the HP Corvalis team for their support with the TIPS system and droplet ejection device. The Purdue University pharmacy dept., in particular, Dr. Pinal for allowing us to use his precision mass balance.

## References

[1] A. K. Sen and J. Darabi , “Droplet ejection performance of a monolithic thermal inkjet print head”, A. K. Sen and J. Darabi , J. Micromech. Microeng., 2007

[2] Alvin U. and Basaran, Osman A., “A new method for significantly reducing drop radius without reducing nozzle radius in drop-on-demand drop production”, Chen, Alvin U. and Basaran, Osman A., Physics of Fluids, 2002

[3] W. Boley, T. Bhuvana, B. Hines, R.A. Sayer, G. Chiu, T.S. Fisher, D. Bergstrom, R. Reifenberger, and G.U. Kulkarni, "Inkjet Printing Involving Palladium Alkanethiolates and Carbon Nanotubes Functionalized with Single-Strand DNA," in the Proceedings of the DF2009: Digital Fabrication Processes Conference, September 20-24, 2009

[4] T. Bhuvana, W. Boley, B. Radha, B. Hines, G. Chiu, D. Bergstrom, R. Reifenberger, T.S. Fisher, and G.U. Kulkarni, "Inkjet Printing of Palladium Alkanethiolates for Facile Fabrication of Metal Interconnects and SERS Substrates." Micro & Nano Letters, Vol. 5, Iss. 5, pp. 296-299, 2010.

[5] Boley, J. W., C. Shou, P. McCarthy, T. Fisher, and G. T.-C. Chiu, "The Role of Coalescence in Inkjet Printing Functional Films: An Experimental Study" in the Proceedings of the DF/NIP29 the International Conference on Digital Printing Technologies, 2013.

[6] Boley, J. W. (2013). “Print mask design for inkjet functional printing”, Purdue University.

[7] Castrejón-Pita, J. R., Morrison, N. F., Harlen, O. G., Martin, G. D., and Hutchings, I. M. ,“Experiments and Lagrangian simulations on the formation of droplets in drop-on-demand mode”, Phys. Rev. E 83, 2011

[8] Castrejón-Pita, A. A. and Castrejón-Pita, J. R. and Martin, G. D., “A novel method to produce small droplets from large nozzles”, Review of Scientific Instruments. 83, 2012

[9] Chen, Alvin U. and Basaran, Osman A., “A new method for significantly reducing drop radius without reducing nozzle radius in drop-on-demand drop production”, Physics of Fluids 14, 2002

[10] Derby, B., “Inkjet printing ceramics: From drops to solid”, 2543-2550. In Journal of the European Ceramic Society 31, (2011)

[11] Derby, Brian “Inkjet Printing of Functional and Structural Materials: Fluid Property Requirements, Feature Stability”, and Resolution, Annual Review of Materials Research, Vol. 40: 395 -414 (Volume publication date June 2010)

[12] Derby, B. and Reis, N. Inkjet Printing of Highly Loaded Particulate Suspensions. MRS Bulletin, 28, 2003

[13] Derby B., "Inkjet printing of functional and structural materials - fluid property requirements, feature stability and resolution”, Ann Rev Mater Res 2010;40:395-414.

[14] Markus Deserno, “The shape of a meniscus on a straight wall” Fluid,Max-Planck-Institut FurÄ Polymerforschung, Ackermannweg 10, 55128 Mainz, Germany, 2004

[15] Einstein, A. (1906). "Eine neue Bestimmung der Moleküldimensionen". Annalen der Physik 19 (2): 289.

[16] Hongwei Zhou, “Simulation model and droplet ejection performance of a thermal-bubble microejector” , A.M. Gué Laboratoire d’Analyse et d’Architecture de Systèmes (LAAS–CNRS), Université de Toulouse, 7 Avenue du Colonel Roche, 31077 Toulouse Cedex, France, Sensors and Actuators B: Chemical, 2010

[17] Kim, Eunjeong and Baek, Jehyun, “Numerical study on the effects of non-dimensional parameters on drop-on-demand droplet formation dynamics and printability range in the up-scaled model”, Physics of Fluids (1994-present), 24, (2012)

[18] Thomas, D. G.. "Transport characteristics of suspension: VIII. A note on the viscosity of Newtonian suspensions of uniform spherical particles". J. Colloid Sci. 1965

[19] Xu, Qi and Basaran, Osman A., “Computational analysis of drop-on-demand drop formation”, Physics of Fluids (1994-present), 19, 102111 (2007)

[20] Yaw, C. L., William Andrew, Norwich, “Thermophysical Properties of Chemicals and Hydrocarbons”, NY, 2008

[21] Ping-Hei Chen, Wen-Cheng Chen, Pei-Pei Ding, S.H. Chang, “Droplet formation of a thermal sideshooter inkjet printhead”, Department of Mechanical Engineering, National Taiwan University, No. 1, Sec. 4, Roosevelt Rd., Taipei, Taiwan, International Journal of Heat and Fluid Flow, 1998

[22] Vahid Fakhfouri, N. Cantale, G. Mermoud, J. Y. Kim, D. Boiko, E. Charbon, A. Martinoli, and J. Brugger, “Inkjet printing of SU-8 for polymer-based mems a case study for microlenses,” in IEEE MEMS 2008

## Author Biography

*Aaron Fulton received his BS in mechanical engineering from the Purdue University (2013) and is pursuing his M.S. in mechanical engineering at Purdue University (2014). His work has focused on the development of thermal inkjet technologies and functional printing.*